Acta Astronautica 178 (2021) 81–88

Contents lists available at ScienceDirect

Acta Astronautica

journal homepage: www.elsevier.com/locate/actaastro

Array-based digital sun-sensor design for CubeSat application

Konstantin Bolshakov, Fuat Kaan Diriker, Ryan Clark, Regina Lee *, Hugh Podmore

Earth and Space Science Engineering, Lassonde School of Engineering, York University, Canada

ARTICLE INFO

Keywords:
CubeSat
Sun sensor
Attitude determination

ABSTRACT

A Custom-designed, digital sun sensor based on the orthogonal photodiode array is proposed. A well-known application of geometrical aperture mask on light detectors is utilized in a non-conventional design for CubeSat application. The main characteristic of this design is the inclusion of a chirped pattern of slits, while using a digital readout of the photodiode arrays. This pattern is expected to allow greater angle detection accuracy while digital photodiode readout decreases complexity and power consumption. The array-based design approach features low power requirements and simpler readout interface and signal processing when compared to matrix-based approach. The proposed sun sensor design will be demonstrated on DESCENT CubeSat as a part of the technology demonstration payload. The characterization of the prototype sensor shows that the current 5-slit design achieves 0.3-degree accuracy with ±51.5-degree field-of-view (FOV).

1. Introduction

In the last few decades space research has undergone several revolutionary changes. Many space activities (satellite development, space exploration, space tourism, to name a few) have been already privatized and commercially offered. Rapid growth in the commercial space industry has been enabled, in part, by the development of low-cost satellite platforms which may be launched at low-cost as members of "shared" launch services. This significant advancement came alongside advances in micro-electromechanical systems (MEMS) technologies that have boosted the capabilities of small satellites by enabling the integration of critical spacecraft subsystems increasingly smaller packages. Nanosatellites, particularly CubeSats™ are an excellent example of the high degree of miniaturization of modern spacecraft and have been increasingly recognized as valuable tools for demonstrating new technologies in space as well as being an effective means to train space engineering professionals due to their relatively low cost.

One critical subsystem for miniaturized satellites is the Attitude Determination and Control System (ADCS); a CubeSat ADCS comprises multiple miniaturized sensors and actuators which act in concert to control the satellite's orientation. A sun sensor is an integral part of a CubeSat ADCS as well as, although less common, a part of a payload system where the orientation of the sun with respect to the satellite is important for the payload operation. A sun sensor is an optoelectronic device, often based on photodiodes, that requires surface area of the satellite in order to expose the required part to the sun. There are several commercially available sun sensors, many of which are expensive, large-in-size and/or require substantial amount of power to operate for CubeSat-class satellites ([1–5]). In this paper, we provide a review of currently available sun sensor technologies, overview of the proposed low-cost digital sun sensor design and characterization results from the prototype sensor, which will be flown on upcoming DESCENT [6] mission.

2. Digital sun sensor design

2.1. Photo-diode sun sensor design

The simplest form of a sun sensor is the one that relies on the analogue readout of photodiodes. One photodiode is usually placed on each face of the satellite such that the sensor measures the incident light intensity along the axis of each face; each measurement is then converted to a component of the sun vector in the frame of the satellite [7]. The advantages of photodiode-based design are low cost and low mass due to very few components required. This design is often implemented in conjunction with other attitude determination sensors to increase the overall determination accuracy without compromising mass and power budgets [8]. With simple signal processing the accuracy is relatively low. Complex processing algorithms can improve the accuracy significantly, but at a cost of computational power and potentially difficult implementation. The design is becoming less common due to development of small inexpensive sensors with higher accuracy. The field of

* Corresponding author.
E-mail address: reginal@yorku.ca (R. Lee).

https://doi.org/10.1016/j.actaastro.2020.08.005
Received 4 May 2020; Received in revised form 17 July 2020; Accepted 3 August 2020
Available online 1 September 2020

view (FOV) of diode-based sun sensor is theoretically 360°, since the FOV of each sensor overlaps with the neighboring ones. The accuracy of this sensor design ranges significantly depending on the complexity of the processing. Generally, the accuracy of photodiode-based design ranges from 3 to 17° [7,9].

2.2. Solar panel current based sun sensing

An alternative to dedicated photodiodes for light intensity detection is to use solar panels, that are commonly found on even the smallest satellites. The geometry of this design is very similar to the photodiode based one. Each face of the satellite has one or more solar cells mounted. Using a trigonometric relation, the relationship between the current outputs and the incident angle of light can be established [10]. Solar-panel current-based sun sensing is often implemented on small missions that do not allow additional part due to mass or other budget restrictions and projects seeking to reduce weight and cost [10]. The accuracy of solar panel-based sensor, similar to photodiode-based design, range greatly with factors such as Analogue to Digital Conversion (ADC) precision, processing complexity and sensor model [10,11]. Accuracy of a typical solar cell base sun sensor design such as the concept described in Ref. [12,13] is approximately ±3°.

2.3. Quadrant based sun sensor design

The traditional design of a sun sensor is based on a 4-segment photodetector arranged in a 2 by 2 matrix with an aperture mask that has a single slit in the middle. The light passes through the slit resulting in a single spot that covers all 4 segments with varying intensity, which is used to infer the sun angle [14]. The main advantage of the quadrant design is a relatively simple geometry and low cost. The main disadvantage of the quadrant design is low accuracy at wide FOV, albeit it is higher than the previously described designs. The accuracy of the quadrant design and other mask-based design increases with the distance between the detector and the mask. This same distance, h, is inversely proportional to the FOV. It is therefore understood that it is difficult to realize both high accuracy and wide FOV, which is expressed and addressed by Chen and Feng in Ref. [15]. They present a measuring principle for analogue sun sensors and apply it to a prototype based on the quadrant design. The accuracy of similar designs vary from 0.06-degrees to 0.5-degrees [15–18] and FOV in range of ±60-degrees.

2.4. Matrix based sun sensor design

An extension of quadrant-based approach is matrix-based design, where the photodetector part consists of a matrix of photodiodes. The size of each row is typically in hundreds of pixels. An active pixel sensor (APS) such as complementary metal-oxide semiconductor (CMOS) or charge-coupled device (CCD), is used as a light detector. Aperture mask options include single slit, multiple slits, a cross, 'L' shaped and others. The main advantage of the photodiode matrix or image-sensor based design is its potential for high accuracy, which depends on the design of the aperture mask and signal processing. The main disadvantage is the complexity of the implementation. APS image sensors often employ sophisticated digital interfaces that require hardware converters or specialized controllers for processing, or alternatively the analogue value of each of matrix photodiode is read one pixel at a time, which increases the complexity of the processing of the data. Accuracy of these sensors also vary form 0.006-degrees in Ref. [19] and 0.02-degrees [20]. FOV is similar to the previously mentioned design around ±60-degrees.

2.5. Array based sun sensor design

A simplified version of a matrix-based design is a dual-array configuration. The two photodiode arrays are arranged perpendicular to one another and aligned with the spacecraft body frame. This design removes most of the pixels from the matrix, leaving only one row and one column, resulting in a similar configuration that is capable of sensing two-dimensional orientation. Each of the two arrays corresponds to an axis. Similar to the matrix based, this design approach allows the freedom of employing various aperture mask configurations, such as single slit per array, 'L' shaped and multi-slit per array. The main advantage of this design is the potential for high accuracy, similar to the matrix approach, while minimizing the number of pixels used for sensing, hence reducing the power consumption and eliminating the need for complex interfaces or sophisticated data processing. The main disadvantage of the array-based design is the surface area required for implementation. The accuracy of the mask-based designs, including the array-based design, increases with the distance between the detector and the mask, while the FOV decreases with the same distance. Accuracy and FOV are similar to those of quadrant-based designs, ranging from <0.1-degrees to 0.5-degrees [21–28].

In summary, most sun sensors featuring active sensing elements (array of photodiodes of APS) seem to achieve better than 0.5-degree accuracy. While better than 0.1-degree accuracy is reported in some literature, the results are based on simulations and theoretical evaluations rather than on-orbit measurements. In a recent study [20], authors present that "*Nowadays, state-of-the-art Sun sensors for CubeSats have resolutions of about 0.5-degrees, with fields-of-view in the 45- to 90-degrees range.*" The same study also compares the design to "*one of the finest off-the-shelf sensors*" with "*an accuracy of 0.3-degrees.*" Referring to the matrix-based design described in Ref. [24]. In this study, we aimed the proposed array-based Sun sensor design to commercial Sun sensors currently available for CubeSat developers such as NanoSSOC, NSS and SSOC series sensors. More detailed survey of commercial CubeSat Sun sensors is also described in Ref. [29]. NanoSSOC-A60 for example, features a ±60-degrees FOV, with better than 0.5-degree accuracy, dimensions of 27.4 × 14 × 5.9 mm and mass of 4 g. In comparison, the proposed Sun sensor design features ±51.5-degrees FOV, better than 0.3-degree accuracy with dimensions of 23 × 23 × 4 mm and 3 g.

3. Digital array-based sun sensor design

The proposed sun sensor design consists of 2 orthogonal photodiode arrays, each with integrated readout circuits, and an aperture mask with multiple slits assembled on a custom printed circuit board (PCB). The photodetector is a commercially available integrated circuits (IC) with ADC Converters and Serial Peripheral Interface (SPI) communication protocol. In this section we describe each component and design parameters associated with the proposed sun sensor design.

3.1. Aperture mask

A multi-slit aperture provides a pattern of light that consists of several lit and shaded areas. When the pattern moves along the array, each boundary between lit and shaded area provides a point of reference, which are the basis of the incident angle estimation. Specifically, in this work, a pattern of slits based on the chirped cosine function was chosen for multiple slit mask. The light detectors of the proposed sun sensor consist of two photodiode array ICs in orthogonal orientation, which are discussed in more detail in the next section. Since the two detectors are identical, the design of the mask was approached in one dimension. The aperture mask is placed directly on top of the photodetector array chip, such that the center of the pattern is aligned with the center of the diode array. The height of the mask, h, is defined as the distance between the surface of the photodiodes and the bottom surface of the aperture mask (Fig. 1). This conversion is through a simple trigonometric relation $\mathrm{d} = \tan\theta/\mathrm{h}$, where θ represents the desired resolution of the sensor, the distance d the pixel pitch of the photodiode array, leaving the height h as the unknown. In Ref. [15,21], chip was manufactured on the AMS 0.35 μm opto-process with 8 μm pixel pitch. In Ref. [30], Chum and Vojta used the same relation to design a single-slit

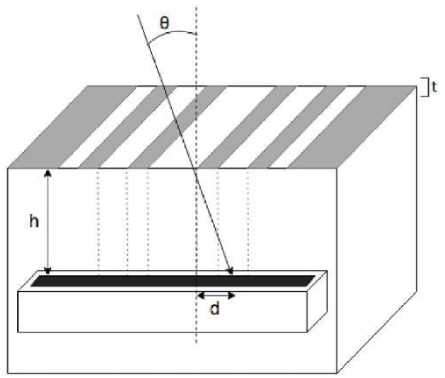

Fig. 1. Conceptual drawing of aperture mask Design.

mask with FOV greater than ±45°.

The focus of the proposed design was to maximize the accuracy while keeping the cost, power consumption and implementation difficulty at their minimum. After considering multiple geometries, the 5-slit design shown in Fig. 2 was selected. The thickness of the mask, t, is defined as the thickness of the slits (Fig. 1). The photo detector selected for the design has $d_{max} = 3.55$ mm; thus, at $h = 2.07$ mm and $t = 0.75$ mm; maximum FOV is estimated to be ±51.5° ($\tan^{-1} d_{max}/(h + t)$). Final design of the 5-slit aperture mask with the fabricated masks (2-axis configurations) are summarized in Table 1 and depicted in Figs. 2 and 3. The 5-slit design is intended to be an error reduction method, especially at lower incidence angles. The center slit is used to calculate the Sun angle and the other slits are used to reduce any readout errors.

3.2. Photo detector and readout electronics

In designing readout electronics for the sensor, several options were considered and an MLX photodetector chip with an internal control and readout circuitry as well as a high-speed ADC was chosen. The control logic of the chip is operated through SPI, which is also used for data transfer. There are multiple modes of ADC operation available on MLX chip: 8-bit, 4-bit, 2-bit and 1-bit. These translate to quantization levels of

Table 1
Proposed sun sensor design summary.

Parameter	Value - units
Pixel Pitch	50 μm
Pixel Size	47 μm
Pixel Count	144
Optical array length	7100 μm
Number of slits	5
Mask dimension (D x W x t)	23 × 23 × 4 mm

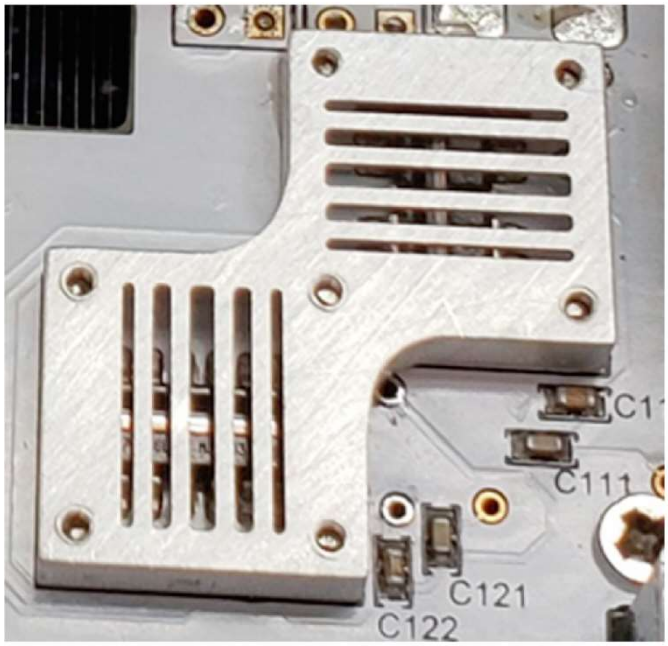

Fig. 3. 2-Axis mask design attached to the Solar Power Payload onboard the DESCENT satellite.

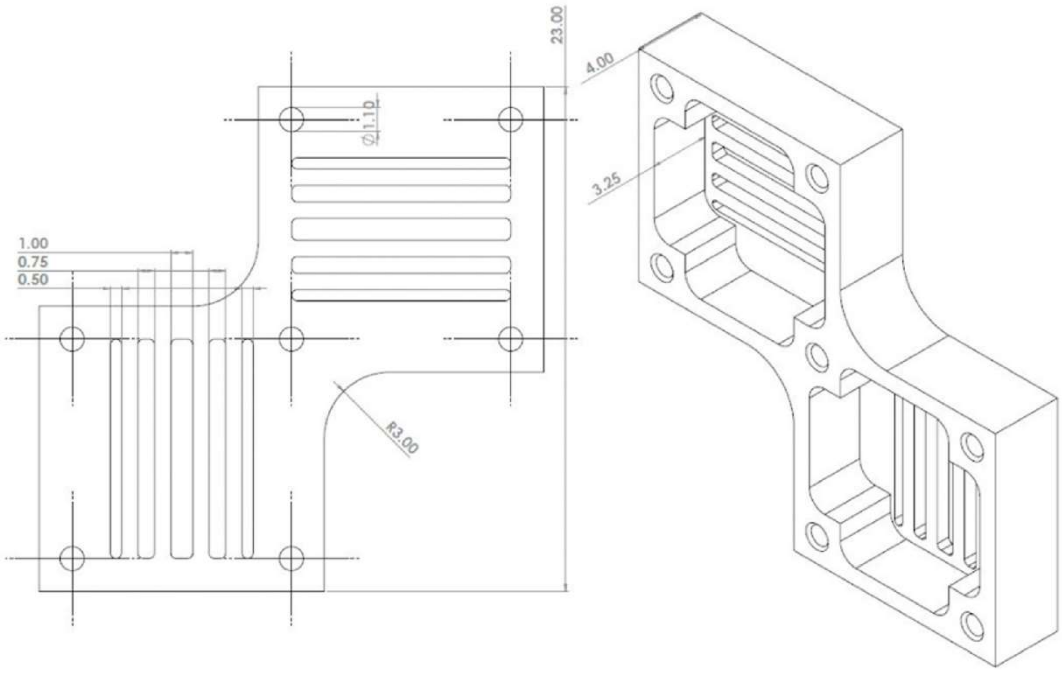

Fig. 2. Front (left) and isometric (right) drawings of the 2-Axis mask design.

the ADC conversion. In 8-bit readout mode, one pixel is represented by 8 bits, which means that one readout of one axis of the sensor will be 142 × 8 = 1136 bits. Since the proposed design is based on a binary pixel readout, 1-bit mode is used. This offloads the computing burden from the microcontroller as well as reduces the size of one readout from 1136 to 142 bits. Data size is an important consideration in satellite design, where the amount of data that can be transferred to the ground is very limited. The data received by the microcontroller is a digital 240-bit string per photodiode array. In this binary string zeros represent no light detected by the corresponding pixels; ones represent that light is detected by the corresponding pixel. For the remainder of the paper, all photo array readouts (zeros and ones) will be represented as a series of dark/lit pixels.

3.3. Simulation study

The performance of the proposed sun sensor design was examined through a simulation study where we produced a series of images between −60 and + 60-degree incident angles. Fig. 5 illustrates the series of photo detector images based on the simulated light conditions with (a) single-slit design and (b) five-slit design.

Each row represents the detector reading at a given incident angle while columns represent the reading of the same pixel at various incident angles.

The sensor algorithm is to interpret the photodetector image to estimate the incident angle. Fig. 4 illustrates the simple geometry used in the calculation. As noted earlier, t denotes the thickness of the mask and h the height of the sensor, and θ the incident angle. X_i is the distance from the edge of the mask to the opening, d_i the location of the pixel where the reading changes from 0 to 1 (for odd number indices) or 1 to 0 (even number indices). Using simple trigonometric relations;

3.4. Field-of-view calculations

In order to get an understanding of the maximum possible field-of-view with the sun-sensor design on 1-bit read readout mode, geometrical calculations were made. Shown in Fig. 4, due to the non-zero thickness of the mask (t), the incidence length $(d_2 - d_1)$ is not equal to slit length $(X_2 - X_1)$. This, along with the length of the photodiode array itself creates the constraints on the field-of-view of the sensors. In order to find the true FOV cone of the sensors, x- and y-axes of the photodiode array were defined on Fig. 4. Geometrical calculations indicate that FOV on the y-axis is ±60.66°. Simulation study shows that the first readings can be taken at ±51.5-degrees on the photodiode x-axis as shown in Fig. 5. This suggests that the lateral FOV is wide enough that there won't be any blind spots between the two photodiode arrays when taking the measurements, and the overall FOV of the sensor can be represented by a 103-degree sensor cone.

3.5. Results and discussion

Fig. 6 illustrates the results of the sun-sensor performance simulation. A series of incidence angles were input to the sun-sensor model generating a set of pixel values for the linear array. The procedure mimics the expected incidence angle retrieval algorithm that would be performed by the sensor on orbit. Over the −51.5° to 51.5-degree range it was found that the retrieval algorithm returned incidence angles with a root-mean-square error (RMSE) of 0.31-degrees (mean error of $\Delta\theta$ = 0.26-degrees) and standard deviation of σ_θ = 0.32-degrees.

4. Sun sensor characterization

4.1. In-lab characterization

The above results were further validated using the in-lab characterization. The laboratory setup used for Sun senor characterization is presented in Figs. 7 and 8. The main components of the setup are the rotation stage, board mount with Sun sensor PCB, light source, and a computer connected to the Sun sensor PCB (not shown on the diagram).

The rotation platform used in this experiment was an Aerotech Inc ARMS Mechanical-Bearing Direct-Drive Rotary Stage, controlled by Soloist Drive-Based Single-Axis Motion Controller. Aerotech Inc. Specifies positioning resolution of up to 0.02 arcsecond and positioning accuracy of ±2.5 arcseconds [31]. The platform is restricted to the single axis of rotation indicated by the arrows above the circular platform on the diagram. The platform has a mark aligned to the center of the mount, while the base has index marks indicating the rotation angle. The board mount was fashioned from a tablet stand and allows for nearly vertical

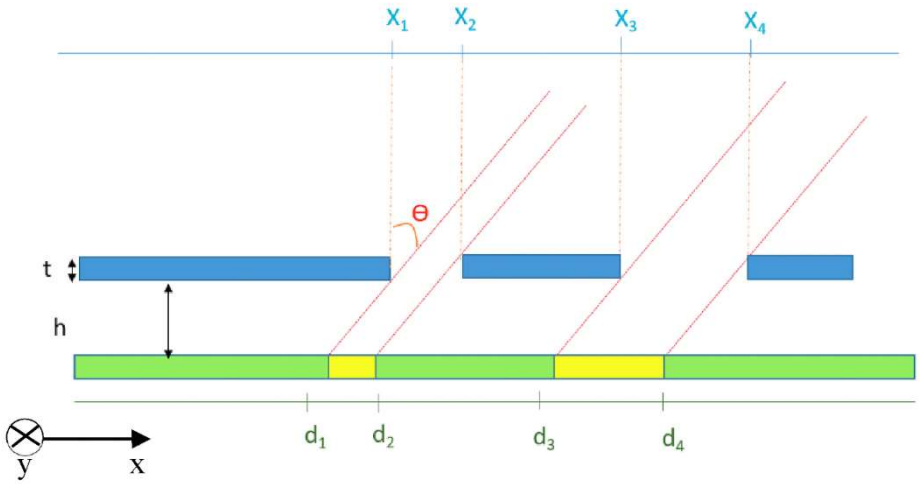

Fig. 4. Parameters used in the sun angle calculation.

$$\theta_i = \tan^{-1}\left(\frac{X_i - d_i}{h}\right) \text{ for } i = 2, 4, 6 \quad (1)$$

$$\theta_i = \tan^{-1}\left(\frac{X_i - d_i}{h + t}\right) \text{ for } i = 1, 3, 5 \quad (2)$$

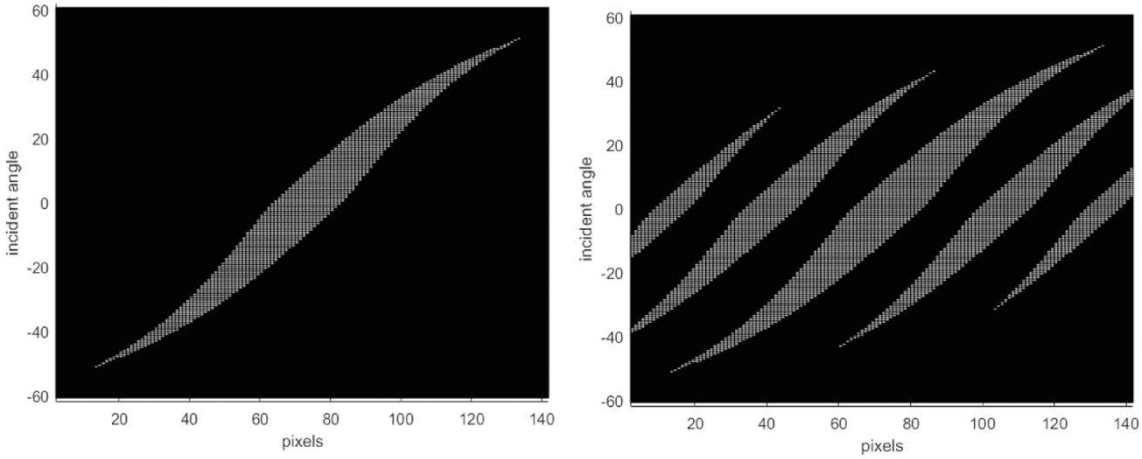

Fig. 5. Simulated incidence pattern images between −60 and 60-degree incident angles using single middle slit (left) and five-slit design (right).

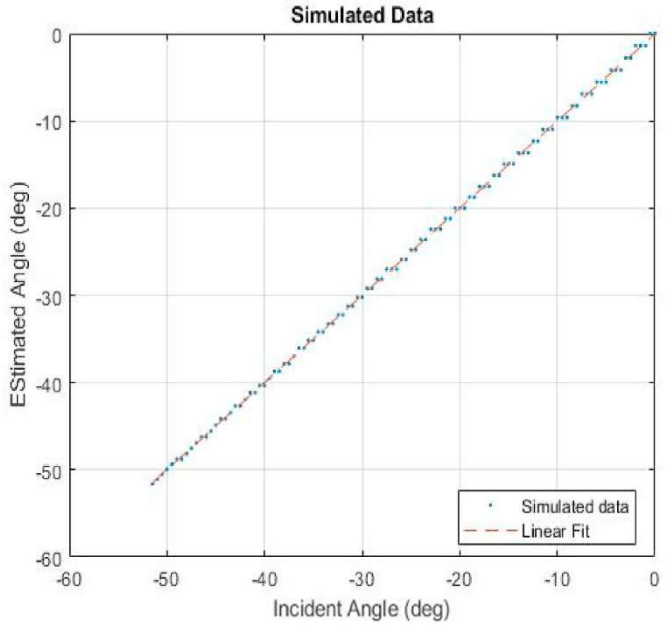

Fig. 6. Estimated vs Calculated angles from the simulated image.

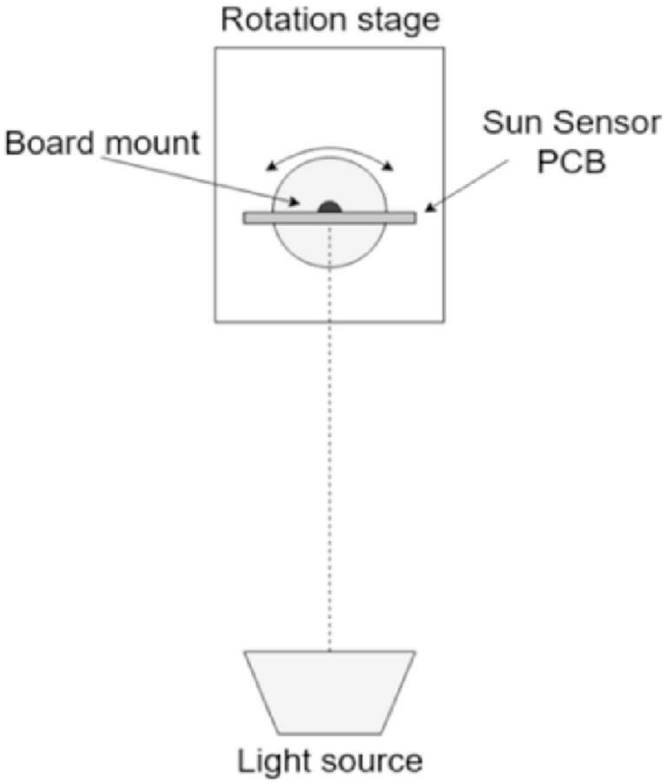

Fig. 7. In-laboratory test setup for Sun sensor characterization (top view).

mounting of the PCB on the rotation stage. The light source used is a portable work light with 300-W bulb. The light bulb used in the experiment had an apparent angular diameter of 3.3° from the sensors. This angular diameter is larger than of the Sun, (0.5-degrees in perihelion) however, due to reflection from the surfaces in the laboratory significantly affected the sensor pattern at longer distances.

To take readings from the sensors, the SPI connection of the PCB was repurposed to interface with the photodiode arrays, while the USART connection initially used to interface with the photodiode arrays was repurposed to act as the serial connection between the PCB and the computer. A testing algorithm developed specifically for this test was flashed into the MCU. The USB port of the computer was driven by a MATLAB software which sent commands to, and received and recorded the measurements from the photodetector arrays. The PCB with the Sun sensor was mounted on the rotational platform such that the center of horizontally oriented photodiode array of the Sun sensor was aligned with the center of the axis of rotation. The horizontal orientation of the PCB was verified with a level. The light source was placed 2 m away from the rotational stage. The platform was set to normal incidence angle (0°) and 10 consecutive readings were taken and recorded. The angle was then changed in increments of 0.5° and 10 measurements were taken for each position until 30° were reached. The same procedure was repeated for the other, negative, side until −30° were reached. The whole procedure was carried out for the second photodiode array, corresponding to the second axis by rotating the PCB 90° and re-mounting it on the platform.

4.2. In-lab characterization results

The test was conducted between −30- and 30-degree range using 5-slit design. The following images illustrate the results from the in-lab characterization tests from −30 to 30°. As in the simulation, the results from −30 to 0-degree is a mirror image of the results from negative side. Similarities between images in Figs. 9 and 10 are evident with a few exceptions. Most notable anomalies from experimental data are the

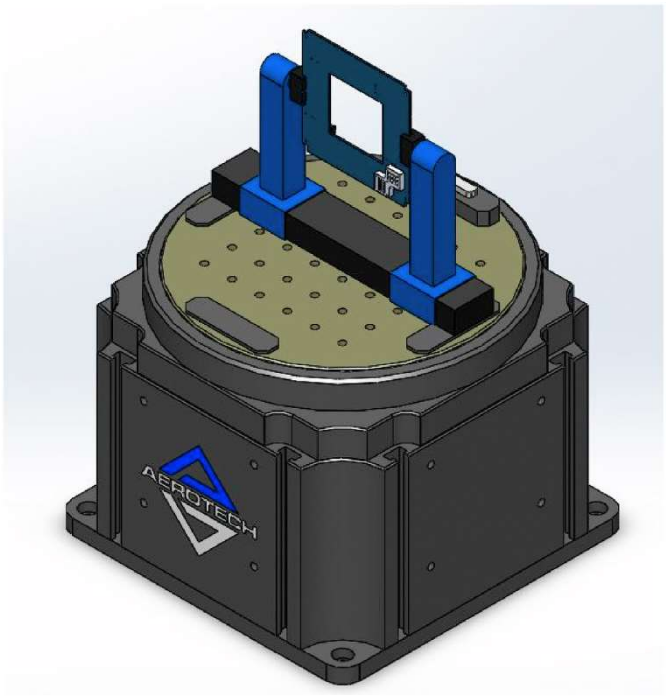

Fig. 8. CAD Model showing the mounting of the PCB on the turntable (isometric).

read-out errors seen at −15, 6, 20, 25 and 30-degree measurements. Also, the pixel #125 is not reading properly indicating dead pixel. Occasional false reading of lit pixel (at -4- or 21-degree incident angles, for example) is also observed.

To improve the accuracy, 10 measurements were taken at each incident angle. For the validation experiment, the mean value of 10 measurements were calculated and used 0.5 as the theshold for lit and unlit pixels. Secondly, single pixel anomalies (one lit pixel inbetween two unlit pixels or the other way around) were removed as read-out noise. Lastly, any significant measurement errors due to reading error (at incident angles −15, 6, etc.) were ignored as outliers. In order to determine if the reading was valid, angle estimation was performed for five slits separately and the reading was considered an outlier if all five angles, θ_i was different from their previous measurement by more than 10°.

In addition to the optical and detector errors (read-out errors and dead pixels described above), there are several sources of errors that could be categorized as "engineering errors". In Ref. [32], four error types are listed as mechanical (manufacturing and alignment), optical and detector (detector and aperture geometry), electrical (signal implication and distortion) and environmental (temperature and radiation). The first three error sources are then compensated through systematic calibration tests. Experimental results (shown in Fig. 11) show that measurements have linear relationship with the incident angles. Further possible error sources are scattering reflection from the work light and non-optimal hardware threshold registers set on the photodiode arrays. For the presented data set above, the linear regression model equation are as follows:

$$\theta_{cal} = \alpha\theta_{meas} \tag{3}$$

$$\theta_{cal} = \alpha\,\theta_{meas} + \beta \tag{4}$$

where θ_{cal} and θ_{meas} represent calibrated and measured incident angles; α and β calibration parameters. For the negative FOV, $\alpha = 1.22$ and $\beta = 4.14°$. Calibration results yield RMSE of 0.33 deg (mean error of $\Delta\theta = 0.28$ deg) after calibration and standard deviation of the error $\sigma_\theta = 0.33$degrees, very similar to the previously predicted error from the simulation studies.

4.3. Future work and hardware calibration

In-lab testing showed differences in numerical and testing data within a reasonable range. The incidence pattern outputted by the testing data was not as smooth and symmetrical as the simulated data, which indicated a need for calibration as outlined in Section 4.2. Future calibration work is to calibrate the hardware of the sensor. The photodiodes placed on the MLX75306 integrated circuits utilize reprogrammable threshold registers. These registers are on-board programmable and can be reprogrammed during the commissioning phase of the flight. Future work includes characterizing the threshold registers and developing an algorithm that can automatically determine and set the appropriate threshold. It is believed that through the usage of these threshold registers that the anomalies seen in the experimental data can be minimized, and the incidence edges can be smoothened to fit with the simulated data.

Currently, there is no estimation of Earth albedo effects on the sun sensor. The calibration steps were able to mitigate the effects of stray light scattering from the surfaces in the laboratory, and the FOV of the aperture mask physically blocks stray light coming from incidence angles greater than 61-degrees (Section 3.4). Combined with the on-board photodiode register thresholding, it is believed that Earth albedo effects can be mitigated in the sensor readings.

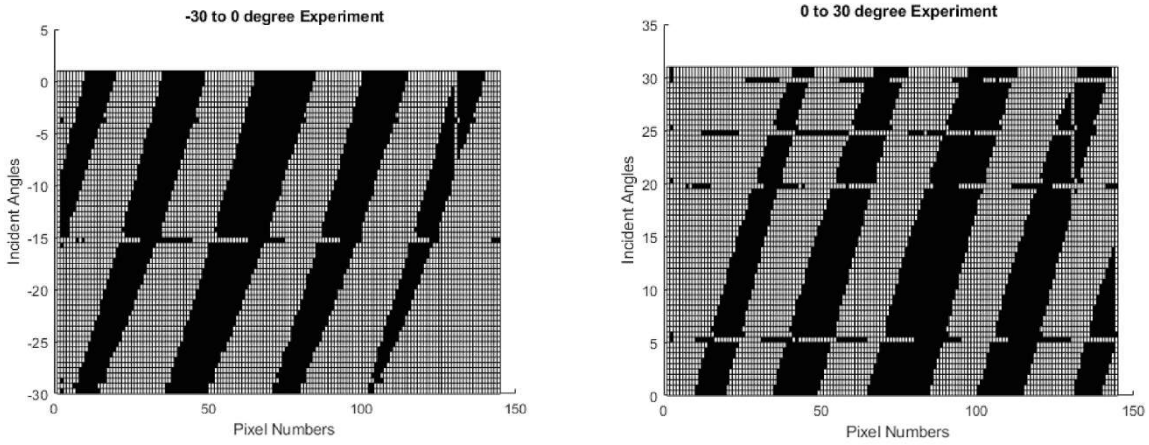

Fig. 9. In-lab Experimental Measurements for X-axis in negative (left) and positive (right) FOV.

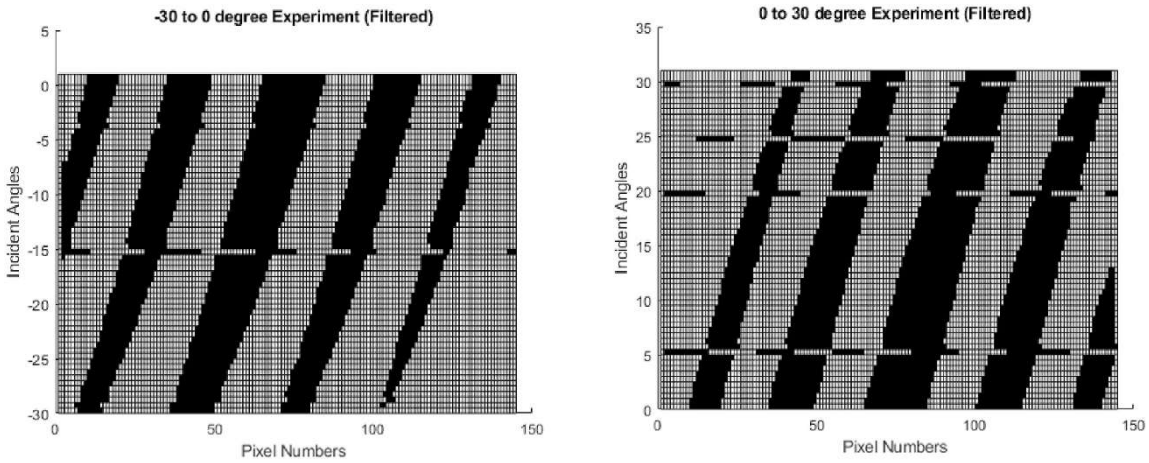

Fig. 10. In-lab Experimental Measurements for Y-axis in negative (left) and positive (right) FOV.

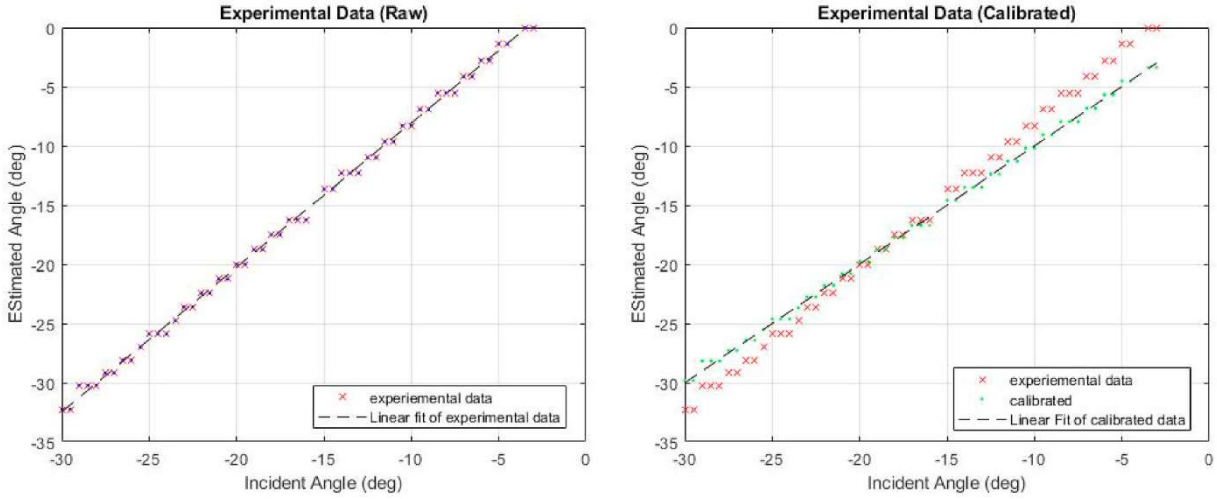

Fig. 11. Calibrated (right) and uncalibrated (left) estimation-incidence plots.

5. Final remarks

A new digital Sun Sensor design has been proposed, formulated, implemented and validated in laboratory environment. The proposed sensor prototype is scheduled to be flown onboard DESCENT CubeSat satellite which has been fully assembled, tested and ready for launch in 2020. As part of the technology demonstration payload, the sun sensor has undergone full environment and functional testing. Once demonstrated on-orbit, this new technology would provide space-qualified products through flight heritage on a CubeSat mission.

Through in-lab characterization tests, we have demonstrated that 0.3-degree accuracy (better than the industry standard of 0.4-degree for digital sun sensors currently available in the market) with careful calibration can be obtained. Along with the accuracy, the sensor exhibits a precision of 0.33-degrees (1σ) and a resolution of 0.5-degrees. In order to realize such ideal measurements, the sensor characterization needs to be developed for post-assembly (after the sensor if mounted on the host satellite) as well as on-orbit procedure during the commissioning phase of the satellite operation. Further accuracy improvements are expected through the implementation of a model-based signal processing or filter, such as Extended Kalman Filter. Additionally, accuracy may be improved by implementing multi-bit read-out of the pixel values, potentially leading to sub-pixel accuracy, however this must be evaluated against the speed and data advantage of binary processing.

Declaration of competing interest

The authors declare that they have no known competing financial interests or personal relationships that could have appeared to influence the work reported in this paper.

Acknowledgements

The authors would like to acknowledge the following sponsors and partners for funding and supporting this project: Natural Sciences and Engineering Research Council of Canada (NSERC) RGPIN-2019-06322, CMC Microsystems, Canadian Space Agency (CSA) 15FASTB09.

References

[1] Nss Fine Sun Sensor, CubeSatShop.com, accessed June 2019, https://www.cubesatshop.com/product/digital-fine-sun-sensor, 2018.
[2] NewSpace Sun Sensor, accessed July 2019, https://www.cubesatshop.com/wp-content/uploads/2016/06/NewSpace-Sun-Sensor_7b.pdf, 2016.
[3] BiSon64-Et-B SunSensor Product Specification Document, BiSon64-ET-B, accessed June 2019, https://lens-rnd.com/sun-sensors/bison64-et-b/, 2018.
[4] nanoSSOC-A60 Technical Specification, Interfaces & Operation, NanoSSOC-A60, accessed June 2019, https://www.cubesatshop.com/wp-content/uploads/2016/06/nanoSSOC-A60-Technical-Specifications.pdf, 2016.
[5] Nss CubeSat Sun Sensor, CubeSatShop, accessed June 2019, https://www.cubesatshop.com/product/nss-cubesat-sun-sensor/, 2016.
[6] V. Jain, U. Bindra, L. Murugathasan, F.T. Newland, Z.H. Zhu, Practical implementation of test-as-you-fly for the DESCENT CubeSat mission, in: 15th

International Conference on Space Operations, 2018, https://doi.org/10.2514/6.2018-2691.
[7] S. Allgeier, M. Mahin, N. Fitz-Coy, Design and analysis of a coarse sun sensor for pico-satellites, in: AIAA Infotech@Aerospace Conference, 2009, https://doi.org/10.2514/6.2009-1837.
[8] J.C. Springmann, J.W. Cutler, Flight results of a low-cost attitude determination system, Acta Astronaut. 99 (2014) 201–214, https://doi.org/10.1016/j.actaastro.2014.02.026.
[9] X. Lü, Y. Tao, K. Xie, S. Wang, X. Li, W. Bao, R. Chen, A photodiode based miniature sun sensor,, Meas. Sci. Technol. 28 (2017), https://doi.org/10.1088/1361-6501/aa61b5.
[10] M. Nygren, J.T. Gravdahl, Using Solar Panels as Sun Sensors on NTNU Test Satellite, Dissertation, Norwegian University of Science and Technology, 2012.
[11] M. Zahran, M. Moawad, A solar cell based coarse sun sensor for a small LEO satellite attitude determination,, Journal of Power Electronics 9 (2009) 631–642.
[12] A. Kocian, E. Cianca, M. Ruggieri, A. Negri, L. Turrini, M. Marino, et al., Analog solar sensor as payload in edusat satellite, in: 2010 IEEE Aerospace Conference, 2010, https://doi.org/10.1109/aero.2010.5446915.
[13] X. Lü, Y. Tao, K. Xie, X. Li, S. Wang, W. Bao, et al., Sun sensor using a nanosatellites solar panels by means of time-division multiplexing, IET Science, Measurement & Technology 11 (2017) 489–494, https://doi.org/10.1049/iet-smt.2016.0352.
[14] I. Maqsood, T. Akram, Development of a low cost sun sensor using quadphotodiode, in: IEEE/ION Position, Location and Navigation Symposium, 2010, https://doi.org/10.1109/plans.2010.5507186.
[15] F. Chen, J. Feng, Analogue sun sensor based on the optical nonlinear compensation measuring principle, Meas. Sci. Technol. 18 (2007) 2111–2115, https://doi.org/10.1088/0957-0233/18/7/042.
[16] D. Faizullin, K. Hiraki, H.-I. Team, M. Cho, Optimization OF a SUN vector determination for pinhole type SUN sensor, Int. J. Regul. Govern. 5 (2017) 436–449, https://doi.org/10.5281/zenodo.838573.
[17] J. Miao, T. Liang, New kind of self-powered wireless digital sun sensor, in: 2017 IEEE 3rd Information Technology and Mechatronics Engineering Conference (ITOEC), 2017, https://doi.org/10.1109/itoec.2017.8122435.
[18] F.J. Delgado, J.M. Quero, J. Garcia, C.L. Tarrida, J.M. Moreno, A.G. Saez, et al., SENSOSOL: MultiFOV 4-Quadrant high precision sun sensor for satellite attitude control, in: 2013 Spanish Conference on Electron Devices, 2013, https://doi.org/10.1109/cde.2013.6481358.
[19] F. Xing, Z. You, G. Zhang, J. Sun, A novel active pixels sensor (APS) based sun sensor based on a feature extraction and image correlation (FEIC) technique, Meas. Sci. Technol. 19 (2008) 125203, https://doi.org/10.1088/0957-0233/19/12/125203.
[20] A. Antonello, L. Olivieri, A. Francesconi, Development of a low-cost sun sensor for nanosatellites, Acta Astronaut. 144 (2018) 429–436, https://doi.org/10.1016/j.actaastro.2018.01.003.
[21] L. Farian, P. Hafliger, J.A. Lenero-Bardallo, A miniaturized two-Axis ultra low latency and low-power sun sensor for attitude determination of micro space probes, IEEE transactions on circuits and systems I, Regular Papers 65 (2018) 1543–1554, https://doi.org/10.1109/tcsi.2017.2763990.
[22] M.A. Post, J. Li, R. Lee, A low-cost photodiode sun sensor for CubeSat and planetary microrover,, International Journal of Aerospace Engineering 2013 (2013) 1–9, https://doi.org/10.1155/2013/549080.
[23] P. Ortega, G. López-Rodríguez, J. Ricart, M. Domínguez, L.M. Castañer, J. M. Quero, et al., A miniaturized two Axis sun sensor for attitude control of nano-satellites,, IEEE Sensor. J. 10 (2010) 1623–1632, https://doi.org/10.1109/jsen.2010.2047104.
[24] B.M.D. Boer, M. Durkut, A low-power and high-precision miniaturized digital sun sensor, Nanophotonics and Macrophotonics for Space Environments VII, 2013, https://doi.org/10.1117/12.2023292.
[25] A. Ali, F. Tanveer, Low-cost design and development of 2-Axis digital sun sensor, J. Spacecraft Technol. 1 (2011).
[26] M. Abhilash, S. Kumar, S. Sandya, T.V. Sridevi, H.R. Prabhamani, Implementation of the MEMS-based dual-axis sun sensor for nano satellites, 2014 IEEE Metrology for Aerospace (MetroAeroSpace), 2014, https://doi.org/10.1109/metroaerospace.2014.6865918.
[27] B.A. Alvi, N. Abbas, A. Israr, M. Asif, Optimized design of sun sensor and centroid algorithm for small satellite mission, in: 2014 4th International Conference on Wireless Communications, Vehicular Technology, Information Theory and Aerospace & Electronic Systems (VITAE), 2014, https://doi.org/10.1109/vitae.2014.6934493.
[28] M.-S. Wei, F. Xing, B. Li, Z. You, Investigation of digital sun sensor technology with an N-shaped slit mask, Sensors 11 (2011) 9764–9777, https://doi.org/10.3390/s111009764.
[29] Carmona Álvaro Enrich, José Camps Carmona Adriano, Sun Sensors for Small Satellites Attitude Determination Systems, dissertation, 2018.
[30] J. Chum, J. Vojta, Wide angle digital slit sun sensor using CCD linear array, in: International Conference on Space Optics — ICSO 2000, 2017, https://doi.org/10.1117/12.2307889.
[31] Arms Mechanical-Bearing Direct-Drive Rotary Stage, Aerotech Inc. (n.d.). https://www.aerotech.com/product-catalog/stages/rotary-stage/arms.aspx?p=%2Fproduct-catalog%2Fstages%2Frotary-stage.aspx%3Fpage (accessed June 23, 2020).
[32] S.-F. Wu, W.H. Steyn, In-orbit modelling and calibration of the sun sensors on UoSat-12 and Tsinghau-1 satellites, in: 15th Annual AIAA/USU Conference on Small Satellites, vol. 3, 2001.